JACS
JOURNAL OF THE AMERICAN CHEMICAL SOCIETY
Article
pubs.acs.org/JACS

Sorption-Induced Structural Transition of Zeolitic Imidazolate Framework-8: A Hybrid Molecular Simulation Study

Liling Zhang,*[,†,‡] Zhongqiao Hu,[‡] and Jianwen Jiang*[,‡]

[†]Jiangsu Key Laboratory for Carbon-Based Functional Materials & Devices, Institute of Functional Nano & Soft Materials, Soochow University, Suzhou, Jiangsu, 215123, China

[‡]Department of Chemical and Biomolecular Engineering, National University of Singapore, 117576, Singapore

Supporting Information

ABSTRACT: A new force field and a hybrid Monte Carlo/molecular dynamics simulation method are developed to investigate the structural transition of zeolitic imidazolate framework-8 (ZIF-8) induced by N_2 sorption. At a high loading (approximately 50 N_2 molecules per unit cell), ZIF-8 shifts from low-loading (LL) to high-loading (HL) structure. A stepped sorption isotherm is predicted with three distinct regions, which agrees well with experimental data. The orientation of imidazolate rings and the motion of framework atoms exhibit sharp changes upon structural transition. Furthermore, pronounced changes are observed in various contributions to potential energies (including stretching, bending, torsional, van der Waals, and Coulombic). The analysis of radial distribution functions between N_2 and framework atoms suggests N_2 interacts strongly with the imidazolate rings in ZIF-8. The simulation reveals that the structural transition of ZIF-8 is largely related to the reorientation of imidazolate rings, as attributed to the enhanced van der Waals interaction between N_2 and imidazolate rings as well as the reduced torsional interaction of framework in the HL structure. This is the first molecular simulation study to describe the continuous structural transition of ZIF-8 and, it provides microscopic insight into the underlying mechanism.

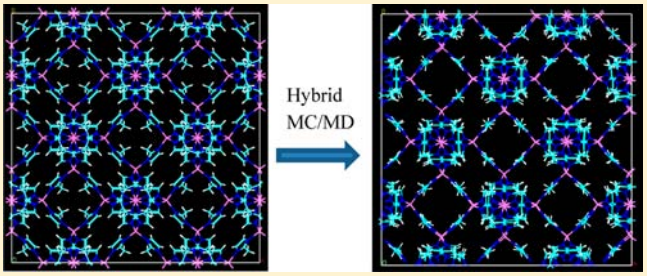

1. INTRODUCTION

As a subfamily of metal−organic frameworks (MOFs), zeolitic imidazolate frameworks (ZIFs) have attracted considerable interest because they possess unique characteristics of both MOFs (e.g., readily tunable structure and functionality) and zeolites (e.g., exceptionally high chemical and thermal stability).[1−4] ZIFs are thus considered as versatile nanoporous materials for a wide range of potential applications, such as shape- and size-selective separation,[5−7] chemical/biochemical catalysis,[8] and drug delivery.[9]

Among a large number of ZIFs synthesized to date, the prototypical ZIF-8 is the most extensively studied. ZIF-8 consists of large cavities (∼ 11.6 Å in diameter) interconnected by narrow six-ring windows. On the basis of experimental single-crystal X-ray diffraction (XRD) data, the window size in ZIF-8 is approximately 3.4 Å.[1] In contrast to zeolites with relatively rigid frameworks, ZIF-8 shows an interesting structural flexibility as evidenced by several experimental studies. For example, gas molecules (N_2, CH_4, C_2H_6, and C_3H_8) with kinetic diameters larger than the window size of ZIF-8 were observed to freely diffuse through ZIF-8.[10−14] Molecular sieving properties of ZIF-8 were examined by a series of probe molecules with increasing kinetic diameter from helium (2.6 Å) to *iso*-C_4H_{10} (5.0 Å), and the effective window size in ZIF-8 was estimated to be between 4.0 and 4.2 Å.[15] Unique stepped sorption behavior was reported for N_2, O_2, CO, and Ar in ZIF-8 at cryogenic temperatures.[16−18] These experiments reveal that the ZIF-8 framework is not completely rigid and may undergo structural transition upon gas exposure. Although the framework flexibility of ZIF-8 is attributed to the swing (reorientation) of imidazolate linkers that enlarges the window size and allows large molecules to enter, the underlying mechanism remains elusive.

In addition to experiments, a handful of simulation studies have been reported on the effects of framework flexibility on gas sorption and diffusion in ZIF-8. From a molecular level, simulation can provide microscopic insight that otherwise is often inaccessible by experimental techniques. Fairen-Jimenez et al. simulated N_2 adsorption at 77 K in two rigid ZIF-8 structures separately, one at ambient pressure[1] and the other at 1.47 GPa,[19] and then suggested N_2 sorption could lead to the structural transition of ZIF-8.[18,20] Haldoupis et al. combined ab initio molecular dynamics (MD) and classical simulation to examine how the framework flexibility would affect gas diffusion in ZIF-8.[21] Alternatively, a few studies attempted to develop force fields to model the framework flexibility of ZIF-8. Hertäg et al. adopted the AMBER and DREIDING force fields to investigate CH_4 diffusion in ZIF-8 and found the crystal structure of ZIF-8 was not accurately predicted, particularly the pore window.[22] These force fields were also used to examine gas diffusion in ZIF-8 by Pantatosaki et al.[23] and Zheng et al.[24] A force field proposed by Battisti et al. predicted the geometrical

Received: January 31, 2013
Published: February 20, 2013

   dx.doi.org/10.1021/ja401129h | J. Am. Chem. Soc. 2013, 135, 3722−3728

parameters of ZIF-8 reasonably well; however, the lack of partial charges restrains its capability primarily for nonpolar molecules.[25] We also developed a force field that can well describe the crystalline, mechanical, and thermophysical properties of ZIF-8, as well as gas diffusion in ZIF-8.[26]

Despite the above-mentioned progress to model the framework flexibility of ZIF-8, to the best of our knowledge, we are not aware of any simulation study that mimics the continuous structural transition of ZIF-8 upon gas sorption. As discussed by Férey and Serre, this phenomenon origins from not only the flexibility and dynamic property of framework, but also gas-framework interaction.[27] It is crucial to fully understand the mechanism governing structural transition, which is useful for important potential applications such as sensing, storage, separation, and drug delivery.

In this study, we develop a new force field and a hybrid simulation method that can describe the continuous structural transition of ZIF-8 upon N_2 sorption and elucidate the underlying mechanism. Following this section, the force field development and simulation methodology are outlined in Section 2. The predictions from the force field are presented in Section 3, including the structural characteristics of ZIF-8, N_2 sorption behavior, and comparison with available experimental data. Finally, the concluding remarks are summarized in Section 4.

2. MODELS AND METHODS

2.1. Force Field. With a cubic sodalite topology, ZIF-8 consists of Zn metals tetrahedrically coordinated by four 2-methylimidazolate (mIM) linkers. Figure 1a illustrates the crystal structure of ZIF-8

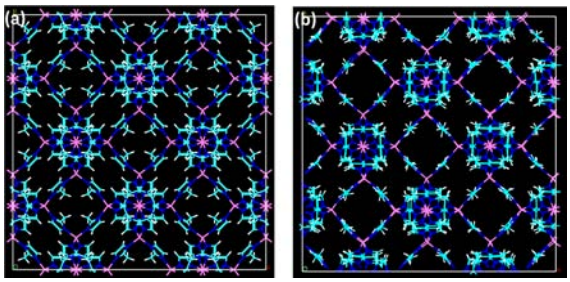

Figure 1. ZIF-8 structures at (a) low loading (LL) and (b) high loading (HL) of N_2 sorption.

experimentally determined at ambient pressure.[1] The atomic types of ZIF-8 are shown in Figure S1 (Supporting Information). To develop the force field for ZIF-8, the parameters in bonded and nonbonded interactions are derived on the basis of the AMBER force field,[28] quantum chemical calculations, and experimental data. The bonded terms include bond stretching and bending, and proper and improper torsional potentials:

$$U_{\text{bonded}} = U_{\text{stretching}} + U_{\text{bending}} + U_{\text{proper}} + U_{\text{improper}} \quad (1)$$

$$U_{\text{stretching}} = \sum \frac{1}{2} k_r (r_{ij} - r_{ij}^0)^2 \quad (2)$$

$$U_{\text{bending}} = \sum \frac{1}{2} k_\theta (\theta_{ijk} - \theta_{ijk}^0)^2 \quad (3)$$

$$U_{\text{proper}} = \sum k_\phi [1 + \cos(m\phi_{ijkl} - \phi_{ijkl}^0)] \quad (4)$$

$$U_{\text{improper}} = \sum k_\xi [1 + \cos(m\xi_{ijkl} - \xi_{ijkl}^0)] \quad (5)$$

where k_r, k_θ, k_ϕ, and k_ξ are the force constants, r_{ij}, θ_{ijk}, ϕ_{ijkl}, and ξ_{ijkl} are bond lengths and angles, proper and improper dihedrals, respectively, m is the multiplicity and was set to two for most dihedrals, and r_{ij}^0, θ_{ijk}^0, ϕ_{ijkl}^0, and ξ_{ijkl}^0 are the equilibrium values, adopted from the averaged bond lengths and angles based on experimental crystallographic data.[1] The parameters for the organic linkers were adopted from the AMBER force field.[28] The challenge here is to describe the coordinative interactions between Zn atoms and organic linkers. There are nine parameters involving Zn atoms, which could be derived by fitting to experimental lattice constants. Specifically, the force constants for the stretching and bending of the tetrahedral ZnN_4 unit (i.e., Zn−N stretching and Zn−N−C1 and Zn−N−C2 bending) were taken from the ad hoc parameters optimized for Zn-containing systems via quantum chemical calculations.[29,30] For N−Zn−N bending and three torsional terms Zn−N−X−Y, where X and Y refer to atoms connected to Zn−N and Zn−N−X, respectively, the force constants in ref 26 were used. It is worthy to note that the accurate description for the dihedrals of N−Zn−N−C1 and N−Zn−N−C2 are crucial to mimic the rotation of imidazolate linkers and the structural transition upon N_2 sorption. These dihedrals were described with multiplicity $m = 3$ and equilibrium values $\phi^0 = 0$, and the force constants were fitted to the experimental data of N_2 sorption isotherm.[18] This is similar to the treatment for the dihedral of X−CT−CT−X in the AMBER force field, where CT is sp^3 hybridized carbon atoms. Tables S1 and S2 (Supporting Information) list the optimized parameters for the bond stretching and bending and the torsional potentials. The force constants involving Zn atoms are generally 1 order of magnitude smaller than those for organic linkers due to the relatively weaker coordination bonds between Zn and N atoms compared to the strong covalent bonds in organic linkers.

The nonbonded interactions include Coulombic and Lennard−Jones (LJ) potentials:

$$U_{\text{nonbonded}} = U_{\text{Coulombic}} + U_{\text{LJ}} \quad (6)$$

$$U_{\text{Coulombic}} = \sum \frac{q_i q_j}{4\pi\varepsilon_0 r_{ij}} \quad (7)$$

$$U_{\text{LJ}} = \sum 4\varepsilon_{ij}\left[\left(\frac{\sigma_{ij}}{r_{ij}}\right)^{12} - \left(\frac{\sigma_{ij}}{r_{ij}}\right)^{6}\right] \quad (8)$$

where q_i is the atomic charge, $\varepsilon_0 = 8.8542 \times 10^{-12}$ C^2 N^{-1} m^{-2} is the vacuum permittivity, and σ_{ij} and ε_{ij} are the collision diameter and well depth, respectively. The atomic charges in ZIF-8 as listed in Table S3 (Supporting Information) were adopted from the plane-wave periodic density functional theory calculations.[31] In most simulation studies for MOFs, the LJ parameters were usually adopted from common force fields such as UFF[32] and DREIDING;[33] however, adsorption in ZIFs was significantly over predicted. In order to match with measured adsorption isotherms, Liu and Smit[34] adjusted the atomic charges and UFF parameters for ZIFs. Separately, Pérez-Pellitero and Battisti rescaled the UFF parameters as $\varepsilon = 0.69\varepsilon_{\text{UFF}}$ and $\sigma = 0.95\sigma_{\text{UFF}}$, which could reproduce the experimental data of CH_4 and CO_2 adsorption in ZIFs.[25,35] As illustrated in Figure S2 (Supporting Information), however, these adjusted LJ parameters cannot mimic the stepped adsorption isotherm of N_2 in ZIF-8. To better reproduce such an isotherm, the well depth in this study is rescaled as $\varepsilon = 0.54\varepsilon_{\text{UFF}}$, while $\sigma = 1.0\sigma_{\text{UFF}}$.

N_2 was mimicked as a three-site model with parameters fitted to the experimental properties of bulk N_2.[36] The N−N bond length was 1.10 Å, and a charge of $-0.482e$ ($e = 1.6022 \times 10^{-19}$ C is the elementary charge) was assigned on the N atom, as well as a charge of $+0.964e$ at the center-of-mass (COM). In addition, the sorption of CO_2 and CH_4 in ZIF-8 was also simulated to further validate the developed force field for ZIF-8. The charges on C and O atoms were $+0.576e$ and $-0.288e$, respectively.[37] The C−O bond length was 1.18 Å, and the bond angle ∠OCO was 180°. CH_4 was represented by a united-atom model interacting with the LJ potential.[38] Table S4 (Supporting Information) lists the LJ potential parameters and the atomic charges for N_2, CO_2, and CH_4. The interactions between sorbates and ZIF-8 were modeled as pairwise additive LJ and Coulombic potentials, and the cross LJ parameters were obtained using the Lorentz−Berthelot combining rules.

dx.doi.org/10.1021/ja401129h | J. Am. Chem. Soc. 2013, 135, 3722−3728

2.2. Simulation. With the force field described above, the crystalline and mechanical properties of ZIF-8 were estimated from MD simulation using DL_POLY (Daresbury Laboratory, Warrington, UK). A system consisting of 8 (2 × 2 × 2) unit cells of ZIF-8 was constructed using the crystal structure at ambient pressure.[1] The lattice constants were predicted from NPT (isothermal−isobaric ensemble) MD simulation at 258 K and 1 atm. Furthermore, the bulk modulus of ZIF-8 was estimated at 298 K. Specifically, NPT MD simulations were conducted at pressures ranging from −0.4 to 0.4 GPa with an interval of 0.1 GPa. A relaxation time of 0.8 ps was used to govern the thermostat and barostat. The equations of motion were integrated with a time step of 1 fs.

Gas sorption in porous materials such as MOFs is generally simulated by the grand canonical Monte Carlo (GCMC) method.[39] Nevertheless, the framework atoms are kept rigid during GCMC simulation. To include framework flexibility in MOFs upon gas sorption, several simulation studies combined GCMC and MD, and the chemical potential/fugacity of sorbate in GCMC was converted to pressure using an equation of state.[40−42] However, a more desirable approach is to examine framework flexibility directly at a given pressure. To achieve this, a hybrid MC and MD simulation method has been developed here for the structural transition of ZIF-8 upon N_2 sorption. Specifically, Gibbs ensemble MC (GEMC) simulation[43,44] was first used to calculate N_2 sorption in rigid ZIF-8 at a given pressure, and then, MD simulation was performed for ZIF-8 loaded with N_2 to relax the ZIF-8 framework; the GEMC/MD simulations were repeated until the sorption capacity converged. In the GEMC simulation, two boxes were used (the first box representing the ZIF-8 framework, and the second box representing bulk N_2). The number of trial moves in the GEMC simulation was 2×10^7, and four types of trial moves were attempted, namely, displacement, rotation, and regrowth in each box, as well as swap between two boxes. After the GEMC simulation, NPT MD simulation was conducted in the first box representing the ZIF-8 framework loaded with N_2. To maintain temperature and pressure, a relaxation time of 0.8 ps was used. The MD simulation was run for 600 ps with a time step of 1 fs. With this hybrid GEMC/MD simulation, the ZIF-8 framework was allowed to relax upon N_2 sorption at a given pressure. At a loading of 50 N_2 molecules/uc (where uc stands for unit cell), structural transition of ZIF-8 was observed from low-loading (LL) to high-loading (HL) structure, as illustrated in Figure 1. The complete isotherm of N_2 at 77 K was simulated using the HL structure as the initial framework with pressure changing from 1 to 0.00001 bar.

3. RESULTS AND DISCUSSION

3.1. Crystalline and Mechanical Properties. On the basis of the developed force field, the crystalline and mechanical properties of ZIF-8 were predicted. Table S5 (Supporting Information) lists the lattice constants as well as typical bond lengths and angles at 258 K and 1 atm. The predicted lattice constants are $a = b = c = 16.981 \pm 0.004$ Å, which agrees well with experimental data ($a = b = c = 16.991 \pm 0.001$ Å)[1] and the deviation is only 0.06%. The bond lengths and angles from the simulation are also in good accord with the measured values, and the deviations are less than 0.4% and 0.9%, respectively. The root-mean squared fluctuations (RMSFs) of ZIF-8 framework atoms are found to fall within 0.3−0.6 Å indicating the ZIF-8 structure is not completely rigid. However, its RMSFs are substantially smaller in contrast to other nanoporous materials (e.g., protein crystals).[45]

The mechanical stiffness of ZIF-8 is quantified by the bulk modulus E_v:

$$E_v = \frac{\sigma_v}{\varepsilon_v} = -V_0 \frac{\partial P}{\partial V} \tag{9}$$

where σ_v and ε_v are the volumetric stress and strain, and V and V_0 are the crystal volumes at actual (P) and reference (P_0) pressures, respectively. Figure S3 (Supporting Information) shows the simulated σ_v versus ε_v, with approximately linear relationship. The estimated E_v is 8.37 ± 0.05 GPa and slightly greater than experimentally determined 6.52 ± 0.35 GPa at low pressures.[46] At high pressures, the experimental stress−strain curve is nonlinear, which is not captured by the force field. Nevertheless, it should be pointed out that accurate prediction of mechanical properties is challenging. For example, a few simulation studies overestimated the bulk modulus of MOF-5 by several-fold.[47−50] The bulk modulus of HKUST-1 from simulation exhibited 17% deviation from the experimental value.[51]

3.2. Structural Transition. As mentioned above, ZIF-8 structure varies from the LL to HL when the number of sorbed N_2 molecules reaches 50/uc. The structural transition is reflected in several aspects, such as the orientation of the imidazolate rings, the motion of the framework atoms, and the N_2 molecules in ZIF-8.

The imidazolate rings in ZIF-8 can be classified into two types. Type I is located at the four-ring window perpendicular to the c axis, while type II refers to the rest of the imidazolate rings. The two types of imidazolate rings differ in orientation. Figure 2 shows the angle (θ) distributions between the normal

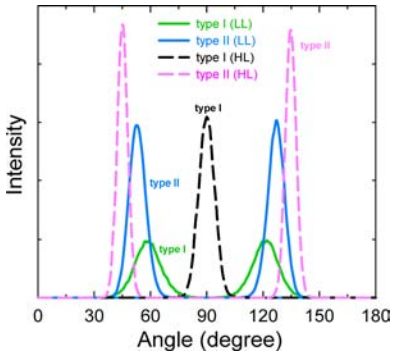

Figure 2. Angle distributions for two types of imidazolate rings in the LL and HL structures of ZIF-8.

vector of the imidazolate ring and the c axis. In the LL structure, θ is centered at 58.8° (or 121.2°) for type I, while at 53.1° (or 126.9°) for type II. The orientation is changed in the HL structure, with type I almost exclusively at 90.0° and type II preferentially at 45.1° (or 134.9°). Such an orientational change can be directly seen from Figure 1. Apparently, the imidazolate rings in the HL structure change orientation being perpendicular to the four-ring window, which is consistent with the experimental XRD data measured at high pressure.[19] Consequently, more space is provided to accommodate sorbed N_2 molecules.

Furthermore, the orientational order of the imidazolate rings is quantified by the order parameter:

$$S = \frac{3}{2}\left\langle \cos^2\theta - \frac{1}{3} \right\rangle \tag{10}$$

Figure 3 plots the evolution of S versus simulation time. At 1.43 ns, sharp variations are observed in the S value for both types I and II imidazolate rings. Specifically, S drops from −0.07 to −0.49 for type I, implying θ changes from 58.8° to 90.0°; and S rises from 0.04 to 0.24 for type II, corresponding to the change of θ from 53.1° to 45.1°. The evolution of the unit cell size of ZIF-8 is plotted in Figure 4. Similar to the order parameter, the cell size exhibits a sharp change from 17.106 to 17.083 Å at 1.43 ns. It should be noted that, when 50 N_2

dx.doi.org/10.1021/ja401129h | J. Am. Chem. Soc. 2013, 135, 3722−3728

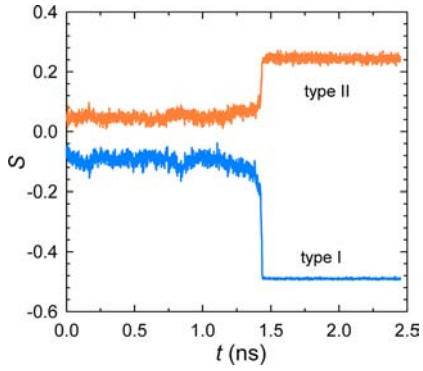

Figure 3. Order parameter versus simulation time for imidazolate rings in ZIF-8 loaded with 50 N_2/uc.

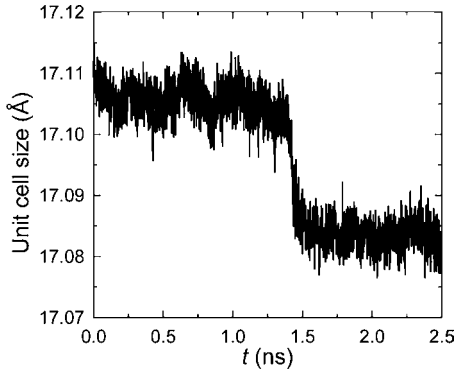

Figure 4. Unit cell size versus simulation time for ZIF-8 loaded with 50 N_2/uc.

molecules were loaded into the LL structure of ZIF-8, the cell size rapidly increased to approximately 17.10 Å and then was maintained for several nanoseconds until transition occurs.

The motions of the framework atoms and N_2 molecules in ZIF-8 are characterized by mean-squared displacement (MSD):

$$\mathrm{MSD}(t) = \frac{1}{N}\sum_{i=1}^{N}\langle|\mathbf{r}_i(t) - \mathbf{r}_i(0)|^2\rangle \quad (11)$$

where N is the number of particles of the same type and $\mathbf{r}_i(t)$ is the position of particle i at time t. As shown in Figure 5, the C2 and Zn atoms in the ZIF-8 framework exhibit small MSD before 1.43 ns. After 1.43 ns, however, the MSD of C2 atoms increases drastically and is more significant than that of Zn atoms. Though not shown, the MSDs of all other atoms (C1, C3, H1, and H2) in the organic linkers behave similarly to the C2 atoms, while the N atoms around the ZnN_4 clusters share the same feature as the Zn atoms. This reveals that the motion of the imidazolate rings, rather than the metal atoms, is substantially affected upon structural transition.

Figure 5 also shows the MSD of N_2 at a loading of 50 molecules/uc in ZIF-8. Similar to the C2 and Zn atoms, a pronounced increase in the MSD is observed at 1.43 ns. The window size in ZIF-8 from its crystalline structure is approximately 3.4 Å, while the kinetic diameter of N_2 is 3.6 Å. On such a basis, N_2 diffusion would be prohibited in ZIF-8. Due to the flexibility of the imidazolate rings, however, N_2 can pass the narrow window with a low diffusivity in the LL structure. Upon structural transition, the imidazolate rings rotate, and the window size increases. Consequently, N_2 can diffuse faster through the window in the HL structure. Specifically, the diffusivity of N_2 was estimated to be 1.8×10^{-7} cm^2/s in the LL structure and 7.1×10^{-7} cm^2/s in the HL structure, respectively.

From the discussion above, structural transition of ZIF-8 is successfully mimicked using the developed force field. To provide microscopic insight into the underlying mechanism for this transition, Figure 6 plots the potential energies versus the simulation time for ZIF-8 loaded with 50 N_2/uc. Upon structural transition, different magnitudes of changes are observed in various contributions to potential energies. Specifically, the torsional and LJ energies (negatively) decrease by 68.2 and 50.5 kcal/mol, respectively. On the contrary, the Coulombic, bond bending, and stretching energies increase by 10.8, 21.8, and 7.1 kcal/mol, respectively. As a consequence, the total potential energy decreases by 79.1 kcal/mol, as largely attributed to the decrease in the torsional and LJ energies. It can be concluded that the initial LL structure with 50 N_2/uc is not stable and shifts to more stable HL structure due to the decrease in the torsional and LJ energies. Particularly, the rotation of the imidazolate rings changes the Zn-involving dihedral angles (e.g., N−Zn−N−X, where X refers to C1 or C2), increases the window size, and decreases the torsional energy. The (negative) decrease in the LJ energy upon structural transition is due to the enhanced attraction between the ZIF-8 framework and N_2 molecules. This is why the structural transition is induced by N_2 sorption.

3.3. N_2 Sorption. As mentioned, the hybrid GEMC/MD simulation method was developed to simulate the N_2 isotherm in ZIF-8. Figure 7 shows good agreement between simulated and experimental results.[18] More importantly, the steps observed in the experiment are well reproduced by our simulation with three regions. In region I at pressure ≥0.01 bar, the HL structure is stable with more than 46 N_2/uc. In region II at pressure between 0.005 and 0.01 bar, structural transition occurs from the initial

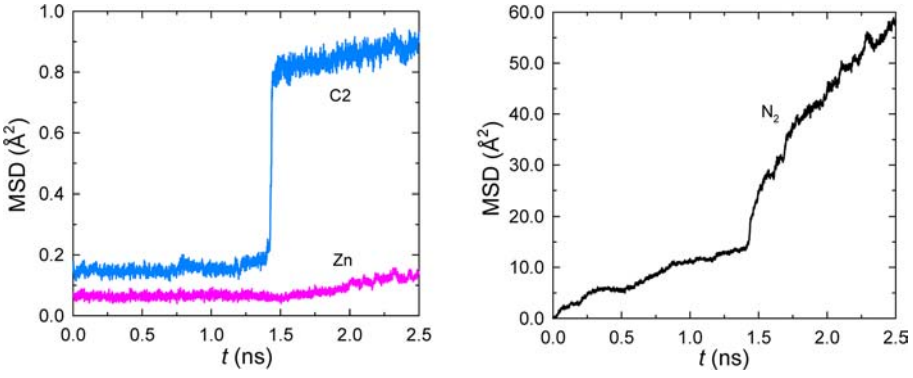

Figure 5. MSDs versus simulation time for the framework atoms and N_2 molecules in ZIF-8 loaded with 50 N_2/uc.

dx.doi.org/10.1021/ja401129h | J. Am. Chem. Soc. 2013, 135, 3722−3728

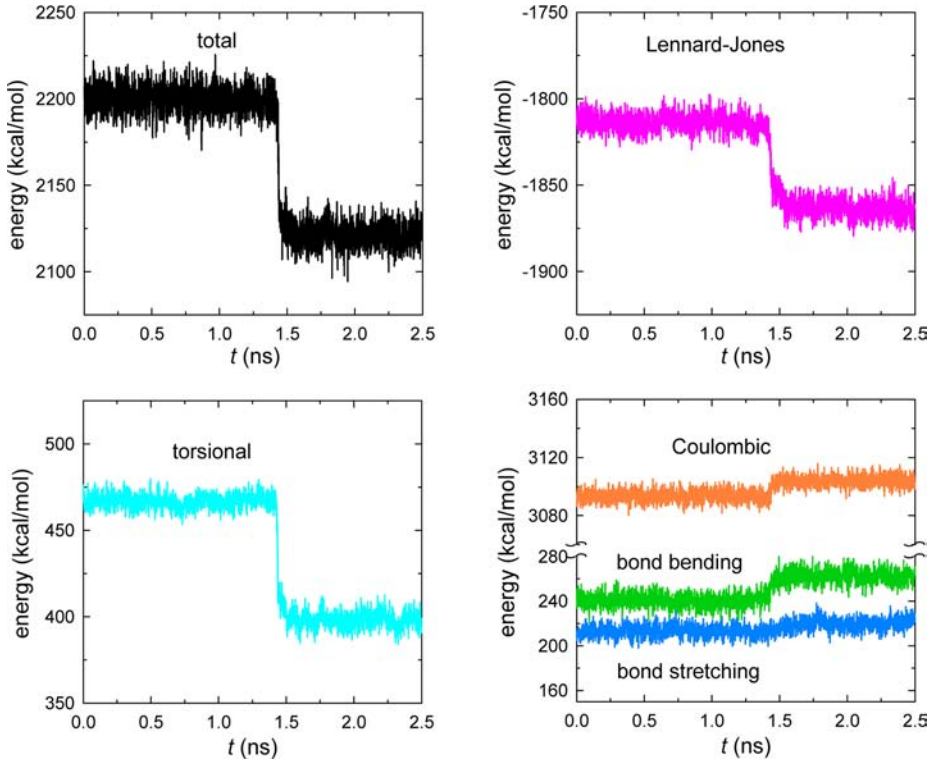

Figure 6. Potential energies versus simulation time for ZIF-8 loaded with 50 N_2/uc.

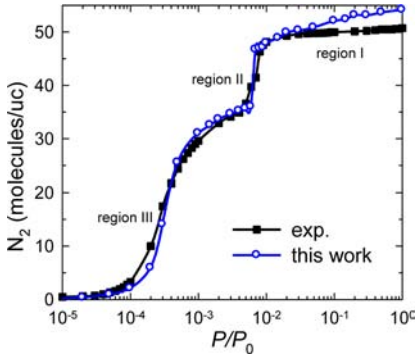

Figure 7. N_2 sorption in ZIF-8 at 77 K versus the pressure of bulk N_2 (P_0 = 1 bar).

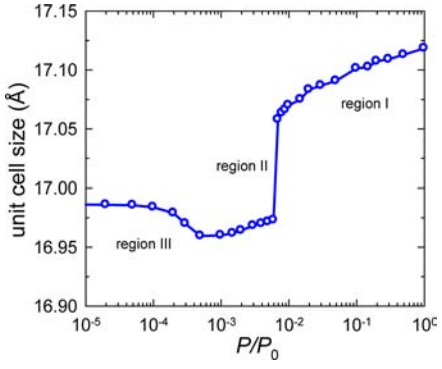

Figure 8. Unit cell size of ZIF-8 versus the pressure of bulk N_2 (P_0 = 1 bar).

HL to the LL structure, corresponding to a decrease of sorbed N_2 from 46.7 to 35.8/uc. In region III at pressure <0.005 bar, the LL structure is stable; therefore, the isotherm is nearly identical to that obtained with the rigid LL structure (see Figure S2, Supporting Information), which further confirms the reliability of the developed force field to reproduce the structural transition of ZIF-8.

As shown in Figure 8, the corresponding unit cell size of ZIF-8 initially reduces with increasing pressure and then slightly rises until the occurrence of structural transition. The initial reduction of cell size is attributed to the internal stress exerted by N_2 sorbed in the framework. Upon structural transition, the cell size rises abruptly. At 1 bar, the size approaches 17.10 Å, which is consistent with the lattice constants of the HL structure at 1.47 GPa.[19] At pressure >1 bar (not shown), the size further increases leading to an increased amount of N_2 sorption.

In order to examine the detailed interactions between N_2 molecules and the ZIF-8 framework, radial distribution functions were calculated by

$$g_{ij}(r) = \frac{N_{ij}(r, r + \Delta r)V}{4\pi r^2 \Delta r N_i N_j} \quad (12)$$

where r is the distance between atoms i and j, $N_{ij}(r, r + \Delta r)$ is the number of atoms j around i within a shell from r to $r + \Delta r$, V is the system volume, and N_i and N_j are the numbers of atoms i and j, respectively. Figure 9 shows the $g(r)$ for N_2 around the Zn, C2, and C3 atoms in ZIF-8 at 0.0003 bar in region III, 0.006 and 0.008 bar in region II, and 1.0 bar in region I, respectively. At 0.0003 and 0.006 bar, a pronounced peak is observed for N_2 around the C2 atoms. This implies N_2 molecules are proximal to the C2═C2 bond of organic linkers located at the pore window, similar to the favorable binding site reported in ZIF-8.[52] With increasing pressure, sharp peaks are seen for N_2 around the C2 and C3 atoms. Therefore, N_2 molecules also interact strongly with the C3 atoms at high pressures (even with C1 atoms though $g(r)$ for C1−N_2 not shown here). This is because the

dx.doi.org/10.1021/ja401129h | J. Am. Chem. Soc. 2013, 135, 3722−3728

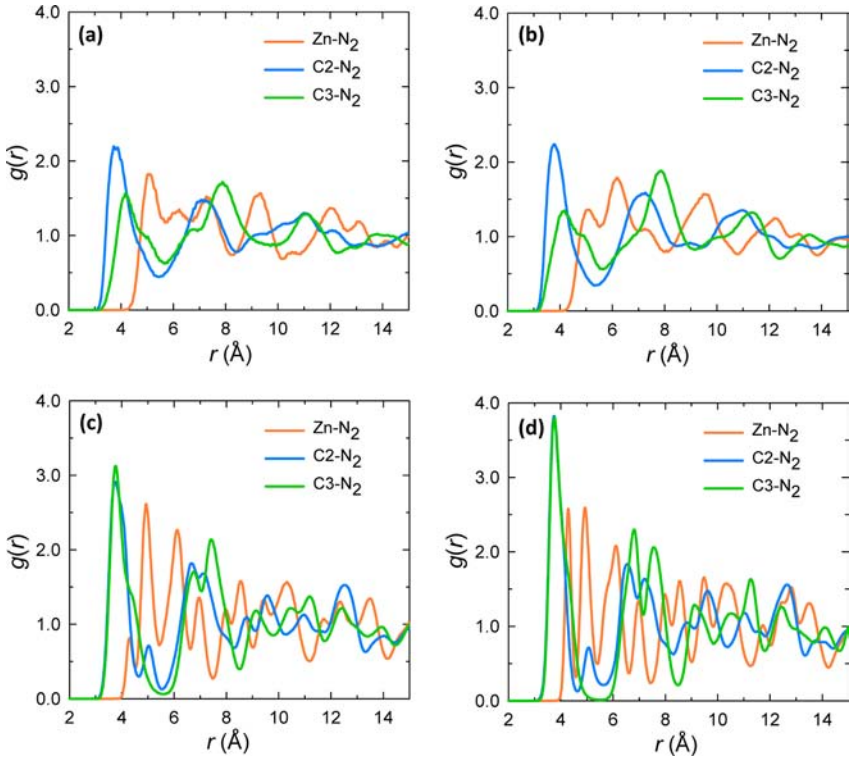

Figure 9. Radial distribution functions for N_2 around the Zn, C2, and C3 atoms in ZIF-8 at (a) 0.0003, (b) 0.006, (c) 0.008, and (d) 1.0 bar.

rotation of the imidazolate rings leads to a larger window and N_2 can be more preferentially sorbed at the window.

Finally, the force field was further used to predict the sorption of CO_2 and CH_4 in ZIF-8 with structural flexibility. As shown in Figure S4 (Supporting Information), the simulated isotherms match well with experimental data at 298 K.[35] This suggests that the force field developed is accurate to describe the sorption behavior of various gases.

4. CONCLUSIONS

In this study, a new force field is developed to describe the framework flexibility of ZIF-8. The predicted crystalline and mechanical properties of ZIF-8 agree well with experimental data. In addition, a hybrid GEMC/MD simulation is developed and combined with the force field to describe the structural transition of ZIF-8 upon N_2 sorption. At a high loading of 50 N_2 molecules/uc, ZIF-8 undergoes structural transition from the LL to HL structure, as accompanied with the reorientation of the imidazolate rings being perpendicular to the four-ring windows. This is attributed to the enhanced van der Waals (Lennard–Jones) interaction between the framework and sorbed N_2 molecules; meanwhile, there is more favorable torsional interaction in the HL structure compared to the LL structure. The transition influences the dynamic motion of the framework atoms and N_2 molecules in ZIF-8. Upon transition from the LL to HL structure, the diffusivity of sorbed N_2 increases by four times. With the developed force field and hybrid simulation method, a stepped isotherm is successfully predicted for N_2 sorption in ZIF-8. Three regions are observed corresponding to the HL structure, the transition from HL to LL, and the LL structure. Furthermore, the radial distribution functions between N_2 and the framework atoms reveal strong interactions between N_2 and the imidazolate rings. This is the first simulation study to mimic the continuous structural transition of ZIF-8 upon N_2 sorption. Microscopic insight into the underlying mechanism is provided from a molecular level. While this study is focused on the prototypical ZIF-8, the force field and hybrid simulation method developed might be extended to other ZIFs and nanoporous materials.

■ ASSOCIATED CONTENT

Supporting Information

Figures showing atomic types of ZIF-8, N_2 adsorption in ZIF-8, volumetric stress versus strain in ZIF-8, and isotherms of CO_2 and CH_4 in ZIF-8; tables showing bond stretching and bending potential parameters in ZIF-8, proper and improper torsional potential parameters in ZIF-8, LJ potential parameters and atomic charges in ZIF-8, N_2, CO_2, and CH_4, and lattice constants, bond lengths, and angles in ZIF-8. This material is available free of charge via the Internet at http://pubs.acs.org.

■ AUTHOR INFORMATION

Corresponding Author

llzhang@suda.edu.cn; chejj@nus.edu.sg

Notes

The authors declare no competing financial interest.

■ ACKNOWLEDGMENTS

The authors gratefully acknowledge the National Science Foundation of China (21173156), the National Basic Research Program of China (973 program, 2012CB932600), the National University of Singapore (R-279-000-297-112), and the National Research Foundation of Singapore (R-279-000-261-281) for financial support.

REFERENCES

(1) Park, K. S.; Ni, Z.; Côté, A. P.; Choi, J. Y.; Huang, R.; Uribe-Romo, F. J.; Chae, H. K.; O'Keeffe, M.; Yaghi, O. M. *Proc. Natl. Acad. Sci. U.S.A.* **2006**, *103*, 10186−10191.
(2) Hayashi, H.; Côté, A. P.; Furukawa, H.; O'Keeffe, M.; Yaghi, O. M. *Nat. Mater.* **2007**, *6*, 501−506.
(3) Banerjee, R.; Phan, A.; Wang, B.; Knobler, C.; Furukawa, H.; O'Keeffe, M.; Yaghi, O. M. *Science* **2008**, *319*, 939−943.
(4) Tan, J. C.; Bennett, T. D.; Cheetham, A. K. *Proc. Natl. Acad. Sci. U.S.A.* **2010**, *107*, 9938−9943.
(5) Banerjee, R.; Furukawa, H.; Britt, D.; Knobler, C.; O'Keeffe, M.; Yaghi, O. M. *J. Am. Chem. Soc.* **2009**, *131*, 3875−3878.
(6) Phan, A.; Doonan, C. J.; Uribe-Romo, F. J.; Knobler, C. B.; O'Keeffe, M.; Yaghi, O. M. *Acc. Chem. Res.* **2010**, *43*, 58−67.
(7) Haldoupis, E.; Nair, S.; Sholl, D. S. *J. Am. Chem. Soc.* **2010**, *132*, 7528−7539.
(8) Tran, U. P. N.; Le, K. K. A.; Phan, N. T. S. *ACS Catal.* **2011**, *1*, 120−127.
(9) Sun, C.-Y.; Qin, C.; Wang, X.-L.; Yang, G.-S.; Shao, K.-Z.; Lan, Y.-Q.; Su, Z.-M.; Huang, P.; Wang, C.-G.; Wang, E.-B. *Dalton Trans.* **2012**, *41*, 6906−6909.
(10) Gücüyener, C.; van den Bergh, J.; Gascon, J.; Kapteijn, F. *J. Am. Chem. Soc.* **2010**, *132*, 17704−17706.
(11) Bux, H.; Chmelik, C.; Krishna, R.; Caro, J. *J. Membr. Sci.* **2011**, *369*, 284−289.
(12) Bux, H.; Chmelik, C.; van Baten, J. M.; Krishna, R.; Caro, J. *Adv. Mater.* **2010**, *22*, 4741−4748.
(13) Li, K.; Olson, D. H.; Seidel, J.; Emge, T. J.; Gong, H.; Zeng, H.; Li, J. *J. Am. Chem. Soc.* **2009**, *131*, 10368−10369.
(14) Bux, H.; Liang, F.; Li, Y.; Cravillon, J.; Wiebcke, M.; Caro, J. *J. Am. Chem. Soc.* **2009**, *131*, 16000−16006.
(15) Zhang, C.; Lively, R. P.; Zhang, K. Z.; Johnson, J. R.; Karvan, O.; Koros, W. J. *J. Phys. Chem. Lett.* **2012**, *3*, 2130−2134.
(16) Aguado, S.; Bergeret, G.; Titus, M. P.; Moizan, V.; Nieto-Draghi, C.; Bats, N.; Farrusseng, D. *New J. Chem.* **2011**, *35*, 546−550.
(17) Ania, C. O.; García-Pérez, E.; Haro, M.; Gutiérrez-Sevillano, J. J.; Valdés-Solís, T.; Parra, J. B.; Calero, S. *J. Phys. Chem. Lett.* **2012**, *3*, 1159−1164.
(18) Fairen-Jimenez, D.; Moggach, S. A.; Wharmby, M. T.; Wright, P. A.; Parsons, S.; Düren, T. *J. Am. Chem. Soc.* **2011**, *133*, 8900−8902.
(19) Moggach, S. A.; Bennett, T. D.; Cheetham, A. K. *Angew. Chem., Int. Ed.* **2009**, *48*, 7087−7089.
(20) Fairen-Jimenez, D.; Galvelis, R.; Torrisi, A.; Gellan, A. D.; Wharmby, M. T.; Wright, P. A.; Mellot-Draznieks, C.; Düren, T. *Dalton Trans.* **2012**, *41*, 10752−10762.
(21) Haldoupis, E.; Watanabe, T.; Nair, S.; Sholl, D. S. *Phys. Chem. Chem. Phys.* **2012**, *13*, 3449−3452.
(22) Hertäg, L.; Bux, H.; Caro, J.; Chmelik, C.; Remsungnen, T.; Knauth, M.; Fritzsche, S. *J. Membr. Sci.* **2011**, *377*, 36−41.
(23) Pantatosaki, E.; Pazzona, F. G.; Megariotis, G.; Papadopoulos, G. K. *J Phys. Chem. B* **2010**, *114*, 2493−2503.
(24) Zheng, B.; Sant, M.; Demontis, P.; Suffritti, G. B. *J. Phys. Chem. C* **2012**, *116*, 933−938.
(25) Battisti, A.; Taioli, S.; Garberoglio, G. *Microporous Mesoporous Mater.* **2011**, *143*, 46−53.
(26) Hu, Z. Q.; Zhang, L. L.; Jiang, J. W. *J. Chem. Phys.* **2012**, *136*, 244703.
(27) Férey, G.; Serre, C. *Chem. Soc. Rev.* **2009**, *38*, 1380−1399.
(28) Duan, Y.; Wu, C.; Chowdhury, S.; Lee, M. C.; Xiong, G. M.; Zhang, W.; Yang, R.; Cieplak, P.; Luo, R.; Lee, T.; Caldwell, J.; Wang, J. M.; Kollman, P. *J. Comput. Chem.* **2003**, *24*, 1999−2012.
(29) Marques, H. M.; Cukrowski, I. *Phys. Chem. Chem. Phys.* **2003**, *5*, 5499−5506.
(30) Lin, F.; Wang, R. *J. Chem. Theory Comput.* **2010**, *6*, 1852−1870.
(31) Rana, M. K.; Pazzona, F. G.; Suffritti, G. B.; Demontis, P.; Masia, M. *J. Chem. Theory Comput.* **2011**, *7*, 1575−1582.
(32) Rappe, A. K.; Casewit, C. J.; Colwell, K. S.; Goddard, W. A.; Skiff, W. M. *J. Am. Chem. Soc.* **1992**, *114*, 10024−10035.
(33) Mayo, S. L.; Olafson, B. D.; Goddard, W. A. *J. Phys. Chem.* **1990**, *94*, 8897−8909.
(34) Liu, B.; Smit, B. *Langmuir* **2009**, *25*, 5918−5926.
(35) Pérez-Pellitero, J.; Amrouche, H.; Siperstein, F. R.; Pirngruber, G.; Nieto-Draghi, C.; Chaplais, G.; Simon-Masseron, A.; Bazer-Bachi, D.; Peralta, D.; Bats, N. *Chem.—Eur. J.* **2010**, *16*, 1560−1571.
(36) Murthy, C. S.; Singer, K.; Klein, M. L.; McDonald, I. R. *Mol. Phys.* **1980**, *41*, 1387−1399.
(37) Jiang, J. W.; Sandler, S. I. *J. Am. Chem. Soc.* **2005**, *127*, 11989−11997.
(38) Martin, M. G. S.; Siepmann, J. I. *J. Phys. Chem. B* **1998**, *102*, 2569−2576.
(39) Jiang, J. W.; Babarao, R.; Hu, Z. Q. *Chem. Soc. Rev.* **2011**, *40*, 3599−3612.
(40) Dubbeldam, D.; Walton, K. S.; Ellis, D. E.; Snurr, R. Q. *Angew. Chem., Int. Ed.* **2007**, *46*, 4496−4499.
(41) Pantatosaki, E.; Megariotis, G.; Pusch, A.-K.; Chmelik, C.; Stallmach, F.; Papadopoulos, G. K. *J. Phys. Chem. C* **2012**, *116*, 201−207.
(42) Ghoufi, A.; Subercaze, A.; Ma, Q.; Yot, P. G.; Ke, Y.; Devic, T.; Guillerm, V.; Zhong, C. L.; Serre, C.; Férey, G.; Maurin, G. *J. Phys. Chem. C* **2012**, *116*, 13289−13295.
(43) Panagiotopoulos, A. Z. *Mol. Phys.* **1987**, *61*, 813−826.
(44) Panagiotopoulos, A. Z. *Mol. Phys.* **1987**, *62*, 701−719.
(45) Hu, Z. Q.; Jiang, J. W. *Langmuir* **2008**, *24*, 4215−4223.
(46) Chapman, K. W.; Halder, G. J.; Chupas, P. J. *J. Am. Chem. Soc.* **2009**, *131*, 17546−17547.
(47) Greathouse, J. A.; Allendorf, M. D. *J. Phys. Chem. C* **2008**, *112*, 5795−5802.
(48) Tafipolsky, M.; Schmid, R. *J. Phys. Chem. B* **2009**, *113*, 1341−1352.
(49) Zhou, W.; Yildirim, T. *Phys. Rev. B* **2006**, *74*, 180301.
(50) Kuc, A.; Enyashin, A.; Seifert, G. *J. Phys. Chem. B* **2007**, *111*, 8179−8186.
(51) Tafipolsky, M.; Amirjalayer, S.; Schmid, R. *J. Phys. Chem. C* **2010**, *114*, 14402−14409.
(52) Wu, H.; Zhou, W.; Yildirim, T. *J. Am. Chem. Soc.* **2007**, *129*, 5314−5316.